Coupled magnetic dipole resonances in sub-wavelength dielectric particle clusters

Mark S. Wheeler,* J. Stewart Aitchison, and Mohammad Mojahedi

The Edward S. Rogers, Sr. Department of Electrical and Computer Engineering, University of Toronto, Toronto, Ontario M5S 3G4, Canada
**Corresponding author: mark.wheeler@utoronto.ca*

Received November 18, 2009; revised February 12, 2010; accepted March 12, 2010; posted March 16, 2010 (Doc. ID 120199); published April 28, 2010

Dielectric spheres which are much smaller than a wavelength and made of a large permittivity can support magnetic dipole modes of great purity. We investigate the coupling of such magnetic dipoles by studying sub-wavelength dielectric spheres arranged in clusters as pairs, chains, and rings. The coupling among the spheres creates hybridized modes, which may be used to engineer metamaterials with more degrees of freedom than by using single particles. Two methods of analysis are used: an approximate coupled dipole model and an exact transition-matrix approach. An experimental setup employs a focused Gaussian beam excitation. The magnetic coupling presented here is similar to the coupling of plasmonic modes in metal nanoparticles. Therefore, these experimental results are also a verification of several analogous plasmonic systems.

OCIS codes: 260.2110, 290.4020, 290.4210, 160.3918.

1. INTRODUCTION

There have been recent reports on magnetic metamaterials made of dielectric spheres. The spheres can have an induced magnetic dipole resonance in the long-wavelength regime if they are made from a material with a very large permittivity, which creates induced magnetic moments in the spheres. A large number of such spheres, possibly as a periodic structure, would acquire a bulk magnetization and an effective permeability. The resonant frequency depends on the sphere material, which might be ferroelectric for microwave resonances [1,2] or dielectric with phonon-polaritonic resonances in the infrared [3–6]. Recent experimental results have been obtained in the microwave range of a negative permeability in a cubic arrangement of ferroelectric cubes [7], as well as a negative index in ferroelectric rods [8]. In the infrared, the magnetic dipole resonance of single isolated SiC whiskers has been observed [9], and the bulk magnetic response of a random powder of SiC micro-particles has been measured [6].

A greater variety and flexibility of metamaterial properties may be obtained by increasing the complexity of the constituents beyond that of single particles. In order to do so, in this paper we consider clusters of particles, which allows near-field coupling within the cluster itself. The particles comprising the clusters will remain spherical. Artificial materials made with clusters for basis units have been studied before, where the clusters are rings of plasmonic spheres having a net magnetic moment [10,11], or arrangements of many metal nanospheres or nanowires into lattices forming larger (but still microscopic) spheres [12] or rods [13]. Such structures have been dubbed *meta-metamaterials* [12]. However, these designs have yet to be validated experimentally.

In this paper we investigate analytically and experimentally the effects of near-field coupling among induced *magnetic* dipoles in sub-wavelength sized clusters of large permittivity spheres. In terms of the dipolar fields external to the spheres, this situation is an exact electromagnetic dual of the electric dipoles induced in plasmonic metal nanoparticles. However, since the underlying physical mechanism is different for the two cases, several distinguishing features can be noted. In the case presented here, the magnetic dipole modes are virtual bulk cavity modes, whereas the modes in plasmonic particles are supported by the electric surface charges, resulting in a uniform internal field. More importantly, however, is that the dispersionless large permittivity spheres used here allow "pure" magnetic dipoles, with negligible contributions by higher multipole terms, whereas plasmonic modes—due to the dispersion of metals—have many spectrally adjacent multipole resonances [14] which can cause additional complexity in the coupled interactions [15]. However, the magnetic dipole interactions studied here remain generally analogous to plasmonic systems, whether in terms of metamaterial properties [10–13], plasmon chemistry [15–17], local-field enhancement [15,18], or waveguiding [19]. Therefore, beyond the intrinsic interest in coupling in sub-wavelength induced magnetic dipole modes, the theoretical and experimental results presented here are important to the study of such plasmonic systems.

The experimental results presented here are in the microwave domain, which simplifies the experimentation. However, the principles of coupling of induced magnetic dipoles in systems of dielectric particles, which are the primary concern of this paper, scale to infrared and optical frequencies; only the specification of the dielectric

functions of the particles would change. We stress that magnetic dipole responses from sub-wavelength sized SiC particles have indeed been measured in the infrared [6,9]. However, it is somewhat difficult to prepare acceptable quality SiC micron-sized spheres and to arrange into precise clusters. To temporarily avoid these difficulties, we present an initial verification of these principles at microwave frequencies, using particles with manageable sizes (~1 mm).

All of the cases studied here, such as pairs, short linear chains, and rings, demonstrate the hybridization of magnetic dipole modes, which is analogous to atomic bonding. While hybridization of plasmonic dipoles, or plasmon chemistry, has been studied before [16,17], the results of hybridized magnetic dipole coupling are novel. In particular, the case of ring clusters presented here demonstrates that different arrangements of bonding create various effective electric or magnetic multipole modes of the cluster, making them useful for the design of metamaterial inclusions. In particular, it is shown and experimentally verified that an effective electric dipole mode is caused strictly by hybridized magnetic dipole coupling (in a circulating loop of displacement magnetic current guided by the spheres), thereby experimentally validating an electromagnetic dual to the idea proposed in [10].

Two analytical methods are applied here. The first is an approximate coupled dipole model (CDM), which is similar to the analysis of coupled electric dipoles in plasmonic spheres [20,21]. Exact calculations are performed using the transition-matrix (T-matrix) approach [22,23], which allows for the calculation of multiple scattering by aggregates of particles [24,25]. The T-matrix approach and similar numerical techniques have been used to study the multiple scattering of systems of particles comparable in size to the wavelength [23,26–29], as well as in plasmonic clusters and chains [15,18,30,31].

This paper is organized as follows. In Section 2 we outline the analytical model and numerical methods used to calculate the normal modes and scattering properties of the clusters of spheres, and we also derive the effective media values from the results. In Section 3 we present the design of our microwave transmission experiments using Gaussian beam principles. The theoretical and experimental results are shown in Section 4, and Section 5 concludes the paper.

2. THEORY

The electromagnetic scattering of a plane wave by an isolated sphere can be calculated using Mie theory [14], which involves decomposing the scattered field into a sum of multipole terms. The magnetic dipole portion of the response is of prominent interest in this work. Consider an isolated sphere of radius r_s, relative permittivity $\varepsilon_s = n_s^2$, and unit relative permeability, in a free-space host ($n_h = 1$). The units will be in SI throughout. The incident plane wave is given by

$$\mathbf{H}^{\mathrm{inc}}(\mathbf{r}) = \mathbf{H}_0^{\mathrm{inc}} \exp(i\mathbf{k}^{\mathrm{inc}} \cdot \mathbf{r}), \tag{1}$$

where $\mathbf{H}_0^{\mathrm{inc}} = H_0\hat{\mathbf{y}}$, $\mathbf{k}^{\mathrm{inc}} = k_0\hat{\mathbf{z}} = (\omega/c)\hat{\mathbf{z}}$ is the incident wavevector, and c is the velocity of light in free space. The magnetic dipole portion of the field scattered by the sphere is proportional to [14]

$$b_1 = \frac{n_h\psi_1(x_s)\psi_1'(x_h) - n_s\psi_1(x_h)\psi_1'(x_s)}{n_h\psi_1(x_s)\xi_1'(x_h) - n_s\xi_1(x_h)\psi_1'(x_s)}, \tag{2}$$

where $x_s = n_s k_0 r_s$, $x_h = n_h k_0 r_s$, $\psi_1(z)$ and $\xi(z)$ are Riccati–Bessel functions, and the primes denote differentiation with respect to the argument. Thus a magnetic dipole moment $\mathbf{m}$ is induced, and the magnetic polarizability α_m of the sphere, defined by $\mathbf{m} = \alpha_m \mathbf{H}_0^{\mathrm{inc}}$, is [4]

$$\alpha_m = \frac{6\pi i}{k_0^3} b_1. \tag{3}$$

For most common materials, the magnetic dipole response b_1 of a sub-wavelength sphere ($\lambda_0/2r_s \gtrsim 10$) is usually 1 order of magnitude smaller than its electric dipole response. There is, however, a situation where a nonmagnetic sphere can have a dominant long-wavelength magnetic response [3–5]. Equating the denominator of Eq. (2) to zero and using the long-wavelength condition $x_h \ll 1$, the resonant frequency f_m of the magnetic dipole resonance is [4]

$$f_m \approx c/2n_s r_s. \tag{4}$$

For sub-wavelength spheres this resonant condition can only be satisfied if the spheres are made of a large permittivity, $\varepsilon_s \gtrsim 100$. In this paper we will consider spheres made of a mixture of oxides, with permittivity $\varepsilon_s = 112 + 0.1i$. For this case, the dominance of the magnetic dipole scattering over the electric dipole and the quadrupole terms can be seen in Fig. 1. Thus such a sphere to a good approximation acts as a magnetic dipole, for the frequency range roughly between 11 and 15 GHz.

A. Coupled Ideal Magnetic Dipoles

When two or more spheres are closely spaced, they may interact strongly. Since our sub-wavelength dielectric spheres approximate ideal electrodynamic magnetic di-

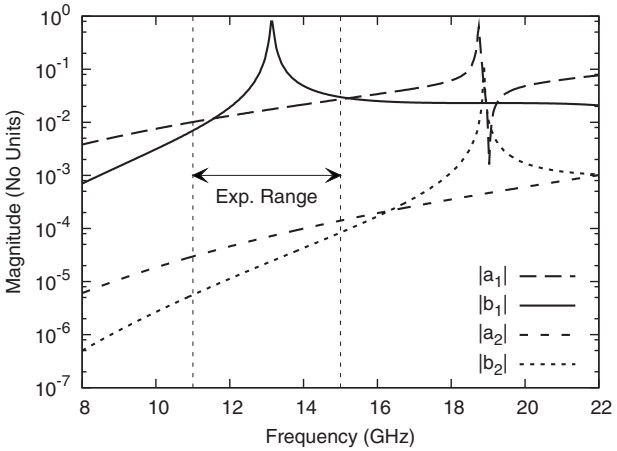

Fig. 1. Magnitudes of the Mie scattering coefficients of a dielectric sphere, having radius $r_s = 1.07$ mm, permittivity $\varepsilon_s = 112 + 0.1i$, and unit permeability. The curves are a_1 electric dipole, b_1 magnetic dipole, a_2 electric quadrupole, and b_2 magnetic quadrupole. The magnetic dipole is dominant throughout the range of frequencies used in the experimental results, 11–15 GHz.

poles, a cluster of such spheres can be modeled by a system of linear equations. We will use the equations to estimate the resonant frequencies, normal modes, and extinction cross sections.

The magnetic field radiated by a magnetic dipole is [32]

$$\mathbf{H}(\mathbf{r}) = \frac{e^{ik_0 r}}{4\pi}\left[\frac{k_0^2}{r}(\bar{\mathbf{I}} - \hat{\mathbf{r}}\hat{\mathbf{r}}) + (3\hat{\mathbf{r}}\hat{\mathbf{r}} - \bar{\mathbf{I}})\left(\frac{1}{r^3} - \frac{ik_0}{r^2}\right)\right]\cdot \mathbf{m} = \bar{\mathbf{G}}(\mathbf{r})\cdot\mathbf{m}, \tag{5}$$

where $\bar{\mathbf{G}}(\mathbf{r})$ is the Green's dyadic and $\bar{\mathbf{I}}$ is the identity dyadic. The coordinate origin is the site of $\mathbf{m}$. For a system of N_s spheres, located at $\mathbf{x}_j$ $(1 \le j \le N_s)$, the local field at particle j is

$$\mathbf{H}^{\mathrm{loc}}(\mathbf{x}_j) = \mathbf{H}^{\mathrm{inc}}(\mathbf{x}_j) + \sum_{k\neq j}^{N_s} \mathbf{H}_k(\mathbf{x}_j - \mathbf{x}_k), \tag{6}$$

where $\mathbf{H}_k(\mathbf{r}) = \bar{\mathbf{G}}(\mathbf{r})\cdot\mathbf{m}_k$ is the magnetic field due to the moment $\mathbf{m}_k$ of particle k. The local field at sphere j induces a moment $\mathbf{m}_j = \alpha_m \mathbf{H}^{\mathrm{loc}}(\mathbf{x}_j)$, where α_m is given approximately by Eq. (3). For a cluster of identical spheres Eq. (6) becomes

$$\frac{1}{\alpha_m}\mathbf{m}_j - \sum_{k\neq j}^{N_s} \bar{\mathbf{G}}(\mathbf{x}_j - \mathbf{x}_k)\cdot\mathbf{m}_k = \mathbf{H}^{\mathrm{inc}}(\mathbf{x}_j). \tag{7}$$

These are the master equations for the CDM.

To estimate the resonant frequencies and to evaluate the normal mode patterns, the incident field can be removed by setting the right-hand side of Eq. (7) to zero. As an example, this situation will be evaluated for a linear chain. Since the incident magnetic field is y-polarized, $\mathbf{m}_k = m_k\hat{\mathbf{y}}$. Then the coefficients of $\mathbf{m}_k$ in the homogeneous equivalent to Eq. (7) form the elements of a matrix A,

$$A_{jk} = \begin{cases} 1/\alpha_m, & j = k \\ -\hat{\mathbf{y}}\cdot\bar{\mathbf{G}}(\mathbf{x}_j - \mathbf{x}_k)\cdot\hat{\mathbf{y}}, & j \neq k \end{cases}. \tag{8}$$

This matrix is frequency dependent, so a straightforward way to find the resonant modes is to sweep the frequency, each time of diagonalizing the matrix. The eigenvectors are hybridized modes, which represent the cluster as a whole, with no external couplings. The eigenvalues λ are frequency dependent, and frequencies that best satisfy the condition of singularity $\lambda = 0$ are resonant frequencies. The corresponding configuration of the magnetic dipole vectors induced in each sphere is given by the associated eigenvector.

We will also present results for a ring of four identical spheres. In this case there are two components to the magnetic dipole moment of each sphere, so Eq. (7) is comprised of eight equations, and a matrix similar to Eq. (8) can be constructed.

The extinction cross section can be calculated from the optical extinction theorem [23,33]. To do so, we require the vector scattering amplitude,

$$\mathbf{F}(\hat{\mathbf{r}}) = re^{-ik_0 r}\mathbf{H}^{\mathrm{sca}} = \frac{k_0^2}{4\pi}\sum_{j=1}^{N_s}[\mathbf{m}_j - (\mathbf{m}_j\cdot\hat{\mathbf{r}})\hat{\mathbf{r}}]\exp(-ik_0\hat{\mathbf{r}}\cdot\mathbf{x}_j), \tag{9}$$

where $\mathbf{m}_j$ are the solutions of the forced coupled system (7), and $\mathbf{H}^{\mathrm{sca}}$ is the total scattered magnetic field in the far-field approximation. Then the extinction cross section is

$$C_{\mathrm{ext}} = \frac{4\pi}{k_0|\mathbf{H}_0^{\mathrm{inc}}|^2}\mathrm{Im}\{\mathbf{F}(\hat{\mathbf{k}}^{\mathrm{inc}})\cdot\mathbf{H}_0^{\mathrm{inc}}\}. \tag{10}$$

B. Numerical Solution Using the Transition-Matrix Approach

In contrast to the approximate coupled dipole mode, the T-matrix approach is exact in principle; the only limitation is set by the upper limit on the number of multipoles for practical implementation. This method improves upon the coupled dipole method of the previous section because all multipole terms can be included. In this paper the dominance of the magnetic dipole modes (Fig. 1) over all other higher-order multipoles means that this improvement will only be apparent for very closely spaced spheres. The T-matrix approach is generally flexible enough to handle clusters of particles with arbitrary geometry, material composition, and particle shape.

In this approach, all of the fields are expanded in the basis of vector spherical waves about the origin. An incident electric field with amplitude E_0 is expanded as

$$\mathbf{E}^{\mathrm{inc}}(\mathbf{r}) = E_0\ \mathrm{Rg}\ \boldsymbol{\Psi}^T(k_0\mathbf{r})\cdot\mathbf{a}, \tag{11}$$

and a scattered field is expanded as

$$\mathbf{E}^{\mathrm{sca}}(\mathbf{r}) = E_0\boldsymbol{\Psi}^T(k_0\mathbf{r})\cdot\mathbf{f}, \tag{12}$$

where the superscript T denotes vector transposition. The column vectors $\mathbf{a}$ and $\mathbf{f}$ contain the expansion coefficients, and the arrays $\mathrm{Rg}\ \boldsymbol{\Psi}(k_0\mathbf{r})$ and $\boldsymbol{\Psi}(k_0\mathbf{r})$ contain the vector spherical wave basis functions, as elaborated in the Appendix. These basis functions are analogous to atomic orbitals, such that the multipole order $l = 1,2,3,\ldots$ corresponds to the orbital quantum number and $-l \le m \le l$ corresponds to the magnetic quantum number. For numerical calculations the expansions are truncated at $l = l_{\max}$ so that the vectors $\mathbf{a}$ and $\mathbf{f}$, which are henceforth all that are needed to represent the fields, each have $L_{\max} = 2l_{\max}(l_{\max}+2)$ components.

Although the incident field can be arbitrary, we consider only the plane wave (1), whose corresponding electric field has a vector of expansion coefficients $\mathbf{a}$ with the following components:

$$a_{lm}^M = i^{l+1}\sqrt{\pi(2l+1)}(\delta_{m,+1} + \delta_{m,-1}),$$

$$a_{lm}^N = i^{l+1}\sqrt{\pi(2l+1)}(\delta_{m,+1} - \delta_{m,-1}), \tag{13}$$

where δ_{lm} is the Kronecker delta.

The scattering properties of an isolated single particle are completely specified by its one-body matrix $\bar{\mathbf{T}}_1$, where the subscript indicates that there is only a single particle

in the problem. This matrix operates on the incident field vector to produce the scattered field,

$$\mathbf{f} = \overline{\mathbf{T}}_1 \cdot \mathbf{a}. \tag{14}$$

The elements of $\overline{\mathbf{T}}_1$ can be calculated by knowing the size and shape of the particle, as well as the permittivity and permeability of the particle and host [23]. We will only consider spherical particles, for which the matrix is diagonal, such that $f_{lm}^M = -b_l a_{lm}^M$ and $f_{lm}^N = -a_l a_{lm}^N$, where a_l and b_l are the Mie coefficients [14], which describe the amplitudes of electric and magnetic l-multipole scattering, respectively.

Now consider a cluster of N_s particles, located at $\mathbf{x}_j$ $(1 \le j \le N_s)$ as shown in Fig. 2. The scattering by each sphere in isolation is described by $\overline{\mathbf{T}}_1^{(j)}$. The cluster can be modeled by a matrix $\overline{\mathbf{T}}_{\text{clust}}$, such that the total scattered field is

$$\mathbf{f} = \overline{\mathbf{T}}_{\text{clust}} \cdot \mathbf{a}, \tag{15}$$

where

$$\overline{\mathbf{T}}_{\text{clust}} = \sum_{j,k=1}^{N_s} \overline{\mathbf{J}}^{(0,j)} \cdot \overline{\mathbf{T}}_{N_s}^{(j,k)} \cdot \overline{\mathbf{J}}^{(k,0)}. \tag{16}$$

$\overline{\mathbf{J}}^{(j,k)} = \overline{\mathbf{J}}(k_0\mathbf{x}_j - k_0\mathbf{x}_k)$ are regular vector translation matrices, which translate the regular vector spherical waves centered at $\mathbf{x}_j$ from those at $\mathbf{x}_k$ [25]. $\overline{\mathbf{T}}_{N_s}^{(j,k)}$ are scatterer-centered T matrices, which may be calculated from $\overline{\mathbf{T}}_1^{(j)}$ and $\mathbf{x}_j$ for each of the N_s particles using an efficient and numerically stable recursive algorithm [25].

The extinction cross section C_{ext} may be calculated with [25]

$$\begin{aligned} C_{\text{ext}} &= \frac{-1}{k_0^2} \text{Re}\{\mathbf{a}^\dagger \cdot \overline{\mathbf{T}}_{\text{clust}} \cdot \mathbf{a}\} \\ &= \frac{-1}{k_0^2} \sum_{j,k=1}^{N_s} \text{Re}\{\exp[ik_0\hat{\mathbf{z}} \cdot (\mathbf{x}_k - \mathbf{x}_j)]\mathbf{a}^\dagger \cdot \overline{\mathbf{T}}_{N_s}^{(j,k)} \cdot \mathbf{a}\}, \end{aligned} \tag{17}$$

where † is the Hermitian adjoint operator. The second of these expressions is a simplification which is only valid for the particular incident plane wave corresponding to Eq. (1), where the propagation direction is $\hat{\mathbf{z}}$, the electric field is $\hat{\mathbf{x}}$-polarized, and the expansion coefficients $\mathbf{a}$ are as in Eq. (13).

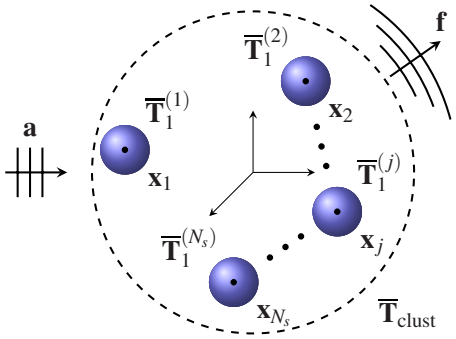

Fig. 2. (Color online) A cluster of N_s particles, bounded by a dashed sphere. Particle j, in isolation, is modeled by $\overline{\mathbf{T}}_1^{(j)}$, and after calculating the multiple scattering solution the cluster within the dashed boundary is modeled by $\overline{\mathbf{T}}_{\text{clust}}$. The incident wave is represented by $\mathbf{a}$, and $\mathbf{f}$ is the total scattered field.

C. Metamaterials with a Cluster Basis

In addition to calculating the scattering of small clusters, we also consider their use as the basis units in a periodic metamaterial. Not only should the spheres be much smaller than a wavelength for this concept to be useful, but so should the cluster itself. The N_s particle cluster, enclosed by a spherical boundary, is shown in Fig. 2. If the cluster has electric and magnetic polarizabilities $\alpha_{e,xx}$ and $\alpha_{m,yy}$, then the effective permittivity $\varepsilon_{r,xx}^{\text{eff}}$ and permeability $\mu_{r,yy}^{\text{eff}}$ of a periodic composite can be found using the Clausius–Mossotti relations,

$$\frac{\varepsilon_{r,xx}^{\text{eff}} - 1}{\varepsilon_{r,xx}^{\text{eff}} + 2} = \frac{N}{3}\left[\frac{1}{\alpha_{e,xx}} + i\left(\frac{k_0^3}{6\pi}\right)\right]^{-1}, \tag{18a}$$

$$\frac{\mu_{r,yy}^{\text{eff}} - 1}{\mu_{r,yy}^{\text{eff}} + 2} = \frac{N}{3}\left[\frac{1}{\alpha_{m,yy}} + i\left(\frac{k_0^3}{6\pi}\right)\right]^{-1}, \tag{18b}$$

where the cluster density is N. The second term in the square brackets, which is not often included in the Clausius–Mossotti relations, cancels the scattering losses included within the polarizability of the first term. Indeed, a periodic metamaterial in the long-wavelength limit should have no scattering losses [34].

The polarizabilities required in Eqs. (18) are proportional to the scattered dipole fields $\mathbf{f}_{1m}$. For example, the magnetic dipole portion of the scattered electric field is transverse to $\hat{\mathbf{r}}$ (TE^r), making it the $f_{1m}^M \mathbf{M}_{1m}(k_0\mathbf{r})$ terms of Eq. (12). This portion of the scattered field can be equated to that from an ideal magnetic dipole [32],

$$\mathbf{E}_{\text{dipole}}^{\text{sca}} = \frac{\eta_0 k_0^3}{4\pi}(\hat{\mathbf{r}} \times \mathbf{m}) h_1^{(1)}(k_0 r), \tag{19}$$

where $\eta_0 = \sqrt{\varepsilon_0/\mu_0}$. The comparison yields

$$\mathbf{m} = -E_0 \frac{\sqrt{3\pi}}{\eta_0 k_0^3}[(f_{1,-1}^M - f_{1,1}^M)\hat{\mathbf{x}} - i(f_{1,-1}^M + f_{1,1}^M)\hat{\mathbf{y}} + \sqrt{2} f_{1,0}^M \hat{\mathbf{z}}]. \tag{20}$$

Since we are considering only the plane wave defined by Eq. (1), the incident magnetic field has only a $\hat{\mathbf{y}}$ component, so the magnetic polarizability $\alpha_{m,yy}$ is

$$\alpha_{m,yy} = \left.\frac{m_y}{H_y}\right|_{H_x = H_z = 0} = \frac{i\sqrt{3\pi}}{k_0^3}(f_{1,-1}^M + f_{1,1}^M). \tag{21}$$

The dual case of the comparison between the TM^r scattered electric dipole field and an ideal electric dipole source yields

$$\alpha_{e,xx} = \left.\frac{p_x}{\varepsilon_0 E_x}\right|_{E_y = E_z = 0} = \frac{\sqrt{3\pi}}{ik_0^3}(f_{1,-1}^N - f_{1,1}^N). \tag{22}$$

These expressions can be verified for the trivial case of a single spherical particle. Then the polarizabilities are scalars, so $\alpha_e = \alpha_{e,xx}$ and $\alpha_m = \alpha_{m,yy}$, and the results match Eq. (3) and the equivalent expression for α_e.

3. EXPERIMENTAL SETUP

A. Gaussian Beam Design

In the theory we have assumed that the clusters are excited by a plane wave. This can be approximated experimentally at microwave frequencies (12–18 GHz) with a pyramidal horn source and a dielectric lens for focusing, as shown in Fig. 3, and a mirror image of the system captures the transmitted signal. The Rexolite biconvex lens is approximately $d_L=7.5$ cm thick along its axis and has a refractive index of $n_L=1.59$. The surface facing the horn has a focal length of $f_1=18.68$ cm corresponding to a radius of $R_1=11$ cm, and the surface facing the sample has a focal length of $f_2=29.00$ cm corresponding to a radius of $R_2=-17.1$ cm.

The shape of a pyramidal horn has been shown to be sufficient to map it into Gaussian optics [35]. The horn aperture dimensions are $w_H=4.29$ cm in the H-plane and $w_E=3.30$ cm in the E-plane, which provide an approximate average beam width at the aperture, $w_a=(0.35w_H+0.5w_E)/2$. The pyramidal slant lengths in each plane are $S_H=10.13$ cm and $S_E=8.36$ cm, which result in an approximate average wavefront radius $R_a=(S_H+S_E)/2$ in the aperture plane.

The beam needs to be focused to a waist where the samples are placed. To approximate a plane wave, there are two requirements. First, to ensure that the field amplitude is uniform over the samples, the beam waist at the sample $w_{0,s}$ must be much larger than the transverse extent of the samples. Second, to ensure that the wavefronts are planar, the Rayleigh range $z_{0,s}$ must be much larger than the longitudinal extent of the samples. In our design we have chosen the distance from the horn aperture to the front of the lens to be $d_1=15$ cm, and simple Gaussian beam principles [36] yield the spacing between the back of the lens and the sample to be $d_2=30$ cm, the beam waist at the sample plane to be $w_{0,s}=2.7$ cm, and the Rayleigh range at the sample to be $z_{0,s}=11.7$ cm. The latter two dimensions are indeed much larger than the samples, ensuring a plane wave excitation.

B. Transmission Measurements

A sample placed at the focused beam waist will scatter power in all directions, the total of which is removed from the incident wave. By the optical theorem, the total of scattering and absorption (which is nearly absent in our samples) is proportional to the extinction cross section C_{ext}. Therefore, the normalized transmittance through the system T_{calc} is the ratio of the intensity measured with the sample in place, I_t, to that with no sample, I_0, which is approximately

$$T_{\text{calc}}=\frac{I_t}{I_0}\approx 1-\frac{C_{\text{ext}}}{A_b}, \tag{23}$$

where $A_b=\pi w_{0,s}^2/0.86$ is the transverse area of the beam at the sample plane and $w_{0,s}$ is the beam waist. The factor of 1/0.86 is due to the definition of the beam width as the $1/e$ distance, so only 86% of the power in the beam is contained within the cylinder defined by the waist.

A sample holder was made from polystyrene foam, which is essentially transparent to microwaves. The horns were connected to an HP 8722C vector network analyzer, allowing for the measurement of the transmission magnitude $|S_{21}|$. The system was calibrated by first saving a measurement of the transmitted powder density $I_0\propto|S_{21}|^2$ without a sample in place. Then a sample was inserted and another measurement was taken $I_t\propto|S_{21}|^2$. The ratio of these measurements yields the normalized transmittance $T_{\text{meas}}=I_T/I_0$, which may be compared with Eq. (23). This process removes the effects of the horns, lenses, and sample holder. Furthermore, 0.2% smoothing and 16 sample averages were used to minimize the noise in these sensitive measurements. The resulting measurements continue to display small ripples, which are likely due to Fabry–Perot reflections between combinations of the lenses and horns. Since the rough extent of the apparatus is on the order of $\Delta d\sim 1$ m, the ripples have a frequency separation [36] on the order of $\Delta f=c/(2\Delta d)\sim 0.15$ GHz.

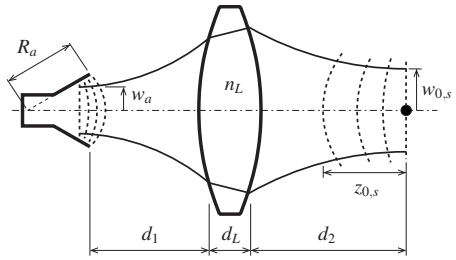

Fig. 3. Schematic of the microwave horn and dielectric lens used to focus a Gaussian beam over a sample sphere. The setup is completed by the mirror image to receive the signal. Some of the curved wavefronts are shown with dashed lines; notice that there is a beam waist within the horn, not at its aperture.

4. RESULTS

The results for three types of arrangements (pairs, chains, and rings) of identical spheres will be presented. The spheres were manufactured by Countis Laboratories (California, USA), from a mixture of $MgO-CaO-TiO_2$. Each sphere has a radius of $r_s=1.07$ mm, permittivity $\varepsilon_s=112+0.1i$, and unit permeability. Using Eq. (4), the estimated magnetic dipole resonant frequency is $f_m\approx 13.2$ GHz, which corresponds to a free-space wavelength of $\lambda_0=2.3$ cm. Thus the host wavelength is about ten times larger than the diameter of a sphere, and the long-wavelength magnetic dipole assumption is valid.

For our T-matrix calculations, we use $l_{\max}=5$. This is chosen based on a measure of uniform convergence, which we define as

$$\Delta_l=\frac{1}{N_f}\sum_{i=1}^{N_f}\left|\frac{C_{\text{ext}}^{l}(f_i)-C_{\text{ext}}^{l-1}(f_i)}{C_{\text{ext}}^{l-1}(f_i)}\right|, \tag{24}$$

where N_f frequency points are evaluated in the range $f_{\min}\le f\le f_{\max}$ so that each frequency is $f_i=f_{\min}+(i-1)\Delta f$ and the frequency step is $\Delta f=(f_{\max}-f_{\min})/(N_f-1)$. This definition provides a notion of convergence over the entire bandwidth of interest. The choice of $l=l_{\max}=5$ guarantees that $\Delta_l\le 10^{-3}$. Note that this value of $l_{\max}$ is significantly smaller than would be expected for the dual case of strongly coupled plasmonic spheres. For example, for only a pair of nearly touching silver nanospheres, a value

$l_{max} > 14$ is required to ensure a similar measure of convergence of $\sim 10^{-2}$ [15], but this is still a factor of 10 weaker than the case presented here. The reason for this difference is that metal spheres have higher-order multipole resonances, as a consequence of the Drude-like dispersion, which satisfy the condition $\varepsilon_s/\varepsilon_0 \approx -(l+1)/l$ [14]. This creates many multipole resonances within a bandwidth adjacent to the dipole resonance, which complicates the strong coupling spectrum.

A. Pair of Spheres

We consider the interaction of two spheres, with various spacings, for two orientations. First, the spheres are spaced on the y axis, which is parallel to the incident magnetic field. Only longitudinal modes will be excited, of which there are two: parallel and anti-parallel dipole moments. Since the direction of propagation is perpendicular to the axis of the pair, the local fields at each sphere must be equal, so only the parallel mode will couple to the incident field. The results for various spacings are shown on the left in Fig. 4. The case of a single sphere is equivalent to two spheres with an infinite spacing. As the spheres are brought together, the parallel-coupled resonance shifts to lower frequencies. The resonant frequency of the anti-parallel mode, as predicted by the theory of Subsection 2.A, is shown by the empty arrowhead, but it is uncoupled due to the orientation of the spheres.

When the spheres are placed on the z axis, only transverse modes are excited. In this case the propagation direction is the same as the pair axis, so there is a phase difference in the incident wave at the two spheres, and their local fields no longer must be equal. Therefore, both the parallel and anti-parallel modes will be excited. The results for various spacings are shown on the right in Fig. 4. What was a single resonance for the isolated sphere splits into two, although in contrast to the previous case, the lower frequency resonance is the anti-parallel mode. The coupled magnetic dipoles interact just like two hybridized of atomic $2p$ orbitals, with bonding and anti-bonding resonances. The more the orbitals overlap due to decreasing separation, the greater the frequency separation of the resonances.

B. Linear Chain of Spheres

We now consider a chain of eight touching spheres, with the same two orientations as in the previous section. The results of the eigenmode analysis from the coupled magnetic dipole theory are shown in Fig. 5. There are eight eigenmode patterns for each polarization case, with the results being essentially the same for each case. The patterns alternate between even and odd, and their eigenfrequencies are ordered oppositely for the two cases.

The transmittance results are shown in Fig. 6. In the case of the longitudinal modes, only four of the eight modes are excited. This is due to the positions of the spheres relative to the incident wave. Since the spheres are placed in a plane of uniform phase of the incident wave, the incident magnetic field is even, so only the even modes are coupled. In the case of the transverse modes, both the odd and even modes can be excited, although some are so weakly coupled that they cannot be distinguished in the transmittance results. Since the spheres are placed along the direction of phase propagation, the incident wave is a frequency-dependent mixture of even and odd modes. In addition, the frequency spread of the resonances is much smaller, so the modes merge into each other and are not easily distinguishable as in the longitudinal case.

C. Ring of Spheres

The normal modes of a ring of four touching spheres are shown in Fig. 7, for the case that the incident electric field is parallel to the ring axis $\hat{\mathbf{x}}$. There are eight modes since there are four spheres and two components of each induced magnetic dipole in the yz-plane. There are doubly degenerate modes at 12.72 and 13.45 GHz.

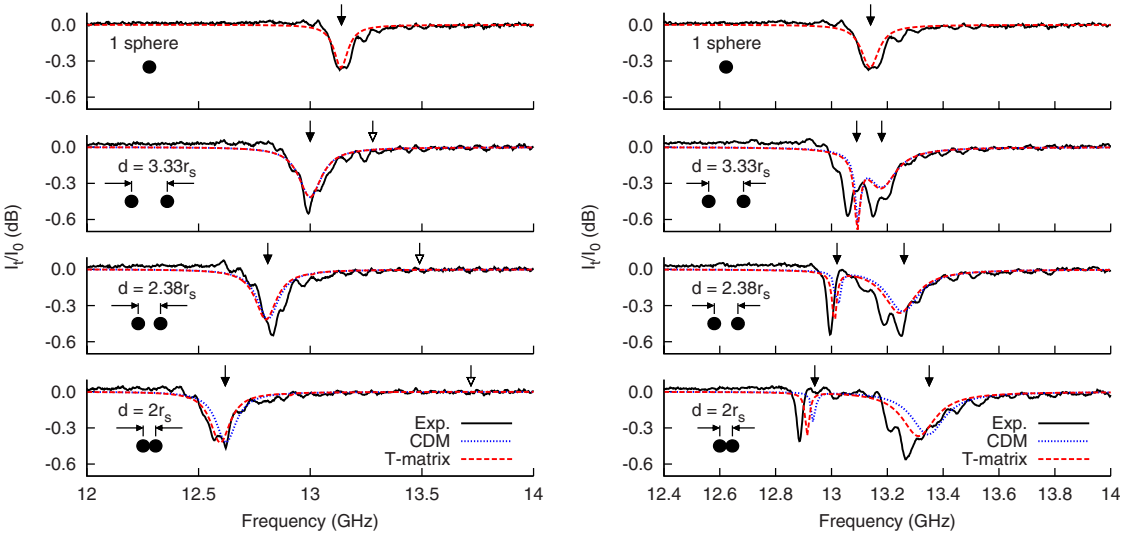

Fig. 4. (Color online) Transmittance through various spacings of paired spheres. On the left are longitudinal modes, where the symmetry axis is parallel to the incident magnetic field, and on the right are transverse modes, where the symmetry axis is perpendicular to the incident magnetic field and parallel to the direction of incident field propagation. The arrows denote the resonant frequencies calculated with the coupled dipole theory, and empty arrowheads indicate uncoupled modes.

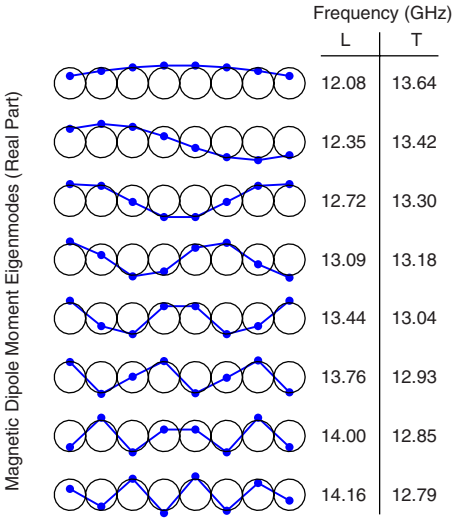

Fig. 5. (Color online) The normal modes of a chain of eight touching spheres, calculated with the coupled magnetic dipole model. The mode frequencies are shown for the longitudinal (L) and transverse (T) polarizations.

The transmittance results for two orientations of the ring are shown in Fig. 8. The results for the two cases are almost the same, with two exceptions: the resonance near 12.63 GHz is uncoupled in the upper configuration, and the resonance near 13.87 GHz is uncoupled in the lower configuration. Each uncoupled mode pattern is orthogonal to the applied excitation. This can be seen by inspecting the mode patterns in Fig. 7 and considering the inner product of $\mathbf{H}^{\text{inc}}$ at each sphere and the dipole patterns. For example, the 12.63 GHz mode is orthogonal to the excitation shown in the inset of the top panel in Fig. 8. However, this mode can couple to the excitation shown in the second panel in Fig. 8.

This ring of touching spheres can be considered as a basis unit of a periodic metamaterial. This is a dual case of the report on a metamaterial made with a ring of plasmonic spheres as a basis, whose individual electric dipole resonances form a circulating electric displacement current and therefore, as a cluster, acts as a magnetic dipole

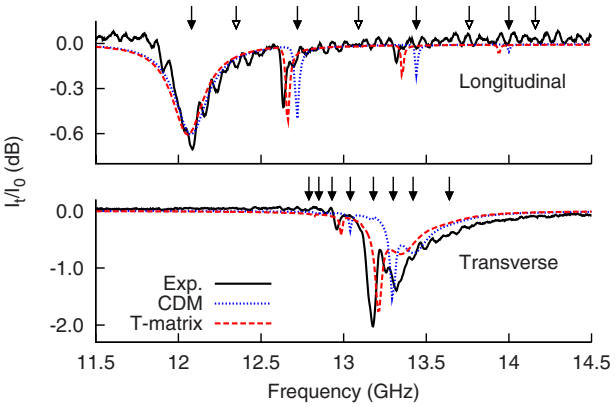

Fig. 6. (Color online) Transmittance through a chain of eight touching dielectric spheres. The top panel is for the chain axis parallel to the incident magnetic field, and the bottom panel is for the chain axis perpendicular to the incident magnetic field (and parallel to the propagation direction). The arrows denote the resonant frequencies calculated with the coupled magnetic dipole theory, and empty arrowheads indicate uncoupled modes.

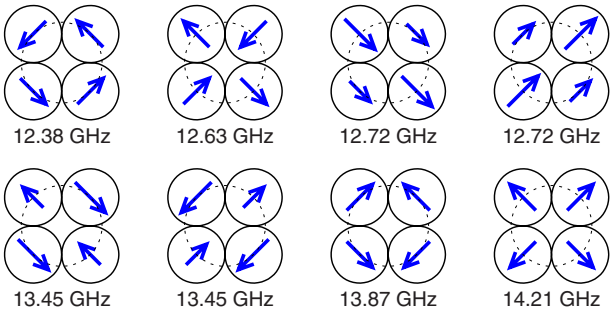

Fig. 7. (Color online) The normal modes of a ring of four touching spheres. The arrows denote the induced magnetic dipole vectors.

which contributes to an effective permeability [10]. However, that report relies on plasmonic spheres with optical resonances, which could prove to be difficult to verify experimentally. Instead, our large permittivity spheres have individual magnetic dipole resonances at microwave frequencies, which can be arranged and measured easily. The lowest frequency cluster mode (Fig. 7) has a circulation of magnetic displacement current, and so it acts as an electric dipole parallel to the ring axis and should contribute to an effective permittivity. We emphasize that this electric dipole resonance is strictly a result of the coupling of the magnetic dipoles among the spheres; it is not possible with a single sphere, where the electric dipole

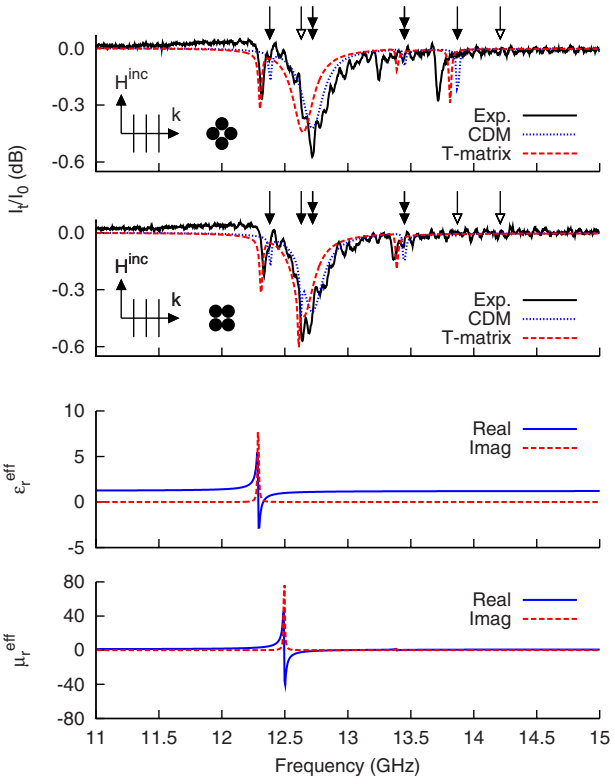

Fig. 8. (Color online) The top two panels show the transmittance through a ring of touching dielectric spheres, for two orientations. The arrows denote the resonant frequencies calculated with the coupled magnetic dipole theory, and empty arrowheads indicate uncoupled modes. The bottom two panels show the calculated effective permittivity and permeability, using the *T*-matrix results, of a periodic metamaterial having the ring as the basis unit.

resonance is at a frequency beyond the experimental range, at 19 GHz (Fig. 1). The doubly degenerate modes near 12.72 and 13.45 GHz both have a net magnetic dipole moment and so should contribute to an effective permeability. The remainder of the modes have no net dipole moments, and although such higher-moment modes may contribute very slightly to the effective media values, they do not enter the simple model of Eq. (18). Having used the coupled magnetic dipole theory of Subsection 2.A for these predictions, we now use the T-matrix results in Fig. 8 and Subsection 2.C to calculate the effective media values of a cubic lattice made with this ring as its basis, where the density of the unit cells is $N=(6\ \text{mm})^{-3}$. The results are shown in the bottom two panels in Fig. 8, and they are the same for both ring orientations since the eigenmodes with a nonzero net magnetic moment are doubly degenerate in the yz-plane. Although there are resonances in both the effective permittivity and permeability, they do not overlap in frequency, and it might be possible to optimize the design to overlap the resonances and create a negative index metamaterial.

Finally, it is interesting to compare the effective electric polarizabilities $\alpha_{e,xx}$ induced by the coupled circulation of magnetic dipoles in the ring to that of a similar single sphere, having the same permittivity as the spheres in the ring, but with a volume equal to the total volume of ring spheres. Thus, the comparison sphere has a radius of 1.70 mm. The result is shown in Fig. 9, where it is seen that the polarizabilities are comparable, and the hybridized mode does not suffer any noticeable coupling loss or broadening. Therefore, such engineered hybridized modes should be useful to create designer molecular-like responses. It is stressed, however, that this comparison is only similar for the effective electric dipole mode of the ring; comparisons of other quantities, such as the cross sections, share few or no similarities.

5. CONCLUSION

We have investigated the coupling of the magnetic dipole resonances of sub-wavelength dielectric spheres with large permittivity. The application of a linear system of coupled ideal magnetic dipoles allows for the prediction of normal mode resonant frequencies and mode patterns, which provide considerable physical insight into the interactions between the spheres. We have also compared the T-matrix and coupled dipole model (CDM) calculations with experimental transmittance results obtained with a focused microwave Gaussian beam setup, and the results match quite closely. Three types of sphere arrangements were studied: pairs of spheres which displayed behavior analogous to the bonding in hybridized atomic orbitals, chains of spheres which are the seed toward subwavelength waveguides, and a ring with an unusual electric dipole response manifested by the coupling of induced magnetic dipoles. The methods and results illustrated here should prove to be useful for studying near-field interactions and higher-moment effects in the fields of metamaterials and plasmonics [17,19,37,38].

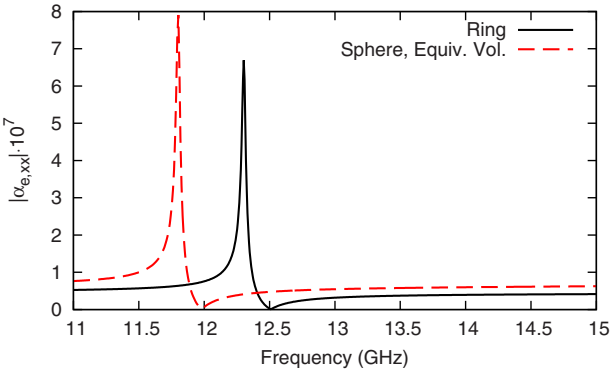

Fig. 9. (Color online) Comparison of the magnitudes of the effective electric polarizabilities of the ring, as arranged in the top panel in Fig. 8, and a single sphere of volume equal to the four spheres comprising the ring.

APPENDIX: VECTOR SPHERICAL WAVES

The fields are expanded in the basis of vector spherical waves, which are grouped into an array using the compact notation [24,39],

$$\boldsymbol{\Psi}^T(k\mathbf{r})\cdot\mathbf{f}=\begin{bmatrix}\mathbf{M}(k\mathbf{r}) & \mathbf{N}(k\mathbf{r})\end{bmatrix}\cdot\begin{bmatrix}\mathbf{f}^M\\ \mathbf{f}^N\end{bmatrix}=\sum_{l=1}^{\infty}\sum_{m=-l}^{l}f_{lm}^M\mathbf{M}_{lm}(k\mathbf{r})+f_{lm}^N\mathbf{N}_{lm}(k\mathbf{r}). \quad \text{(A1)}$$

The basis functions $\mathbf{M}_{lm}$ and $\mathbf{N}_{lm}$ are the irregular vector spherical waves [23,25],

$$\mathbf{M}_{lm}(k\mathbf{r})=-h_l^{(1)}(kr)\mathbf{X}_{lm}(\hat{\mathbf{r}}), \quad \text{(A2a)}$$

$$\mathbf{N}_{lm}(k\mathbf{r})=\frac{1}{kr}\{\sqrt{l(l+1)}h_l^{(1)}(kr)\mathbf{Y}_{lm}(\hat{\mathbf{r}})+[krh_l^{(1)}(kr)]'\mathbf{Z}_{lm}(\hat{\mathbf{r}})\}, \quad \text{(A2b)}$$

where $h_l^{(1)}(z)$ are the spherical Hankel functions. The regular vector spherical waves, denoted by Rg $\mathbf{M}_{lm}$ and Rg $\mathbf{N}_{lm}$, use the spherical Bessel functions $j_l(z)$, instead. The angular dependence of the waves is the normalized vector spherical harmonics [25],

$$\mathbf{Y}_{lm}(\hat{\mathbf{r}})=\gamma_{lm}\sqrt{l(l+1)}P_l^m(\cos\theta)e^{im\phi}\hat{\mathbf{r}}, \quad \text{(A3a)}$$

$$\mathbf{X}_{lm}(\hat{\mathbf{r}})=\gamma_{lm}e^{im\phi}\left[\frac{-im}{\sin\theta}P_l^m(\cos\theta)\hat{\theta}+\frac{\mathrm{d}}{\mathrm{d}\theta}P_l^m(\cos\theta)\hat{\phi}\right], \quad \text{(A3b)}$$

$$\mathbf{Z}_{lm}(\hat{\mathbf{r}})=\gamma_{lm}e^{im\phi}\left[\frac{\mathrm{d}}{\mathrm{d}\theta}P_l^m(\cos\theta)\hat{\theta}+\frac{im}{\sin\theta}P_l^m(\cos\theta)\hat{\phi}\right], \quad \text{(A3c)}$$

where

$$\gamma_{lm}=\sqrt{\frac{(2l+1)(l-m)!}{4\pi l(l+1)(l+m)!}}, \quad \text{(A4)}$$

and $P_l^m(x)$ are the associated Legendre functions.

REFERENCES

1. S. O'Brien and J. B. Pendry, "Photonic band-gap effects and magnetic activity in dielectric composites," J. Phys. Condens. Matter **14**, 4035–4044 (2002).
2. O. G. Vendik and M. S. Gashinova, "Artificial double negative (DNG) media composed by two different dielectric sphere lattices embedded in a dielectric matrix," in *Proceedings of the 34th European Microwave Conference* (IEEE, 2004), Vol. 3, pp. 1209–1212.
3. M. S. Wheeler, J. S. Aitchison, and M. Mojahedi, "Three-dimensional array of dielectric spheres with an isotropic negative permeability at infrared frequencies," Phys. Rev. B **72**, 193103 (2005).
4. M. S. Wheeler, J. S. Aitchison, and M. Mojahedi, "Coated non-magnetic spheres with a negative index of refraction at infrared frequencies," Phys. Rev. B **73**, 045105 (2006).
5. V. Yannopapas and A. Moroz, "Negative refractive index metamaterials from inherently non-magnetic materials for deep infrared to terahertz frequency ranges," J. Phys. Condens. Matter **17**, 3717–3734 (2005).
6. M. S. Wheeler, J. S. Aitchison, J. I. L. Chen, G. A. Ozin, and M. Mojahedi, "Infrared magnetic response in a random silicon carbide micropowder," Phys. Rev. B **79**, 073103 (2009).
7. Q. Zhao, L. Kang, B. Du, H. Zhao, Q. Xie, X. Huang, B. Li, J. Zhou, and L. Li, "Experimental demonstration of isotropic negative permeability in a three-dimensional dielectric composite," Phys. Rev. Lett. **101**, 027402 (2008).
8. L. Peng, L. Ran, H. Chen, H. Zhang, J. A. Kong, and T. M. Grzegorczyk, "Experimental observation of left-handed behavior in an array of standard dielectric resonators," Phys. Rev. Lett. **98**, 157403 (2007).
9. J. A. Schuller, R. Zia, T. Taubner, and M. L. Brongersma, "Dielectric metamaterials based on electric and magnetic resonances of silicon carbide particles," Phys. Rev. Lett. **99**, 107401 (2007).
10. A. Alù, A. Salandrino, and N. Engheta, "Negative effective permeability and left-handed materials at optical frequencies," Opt. Express **14**, 1557–1567 (2006).
11. A. Alù and N. Engheta, "Dynamical theory of artificial optical magnetism produced by rings of plasmonic nanoparticles," Phys. Rev. B **78**, 085112 (2008).
12. C. Rockstuhl, F. Lederer, C. Etrich, T. Pertsch, and T. Scharf, "Design of an artificial three-dimensional composite metamaterial with magnetic resonances in the visible range of the electromagnetic spectrum," Phys. Rev. Lett. **99**, 017401 (2007).
13. W. Park and Q. Wu, "Negative effective permeability in metal cluster photonic crystal," Solid State Commun. **146**, 221–227 (2008).
14. C. F. Bohren and D. R. Huffman, *Absorption and Scattering of Light by Small Particles* (Wiley, 1983).
15. R.-L. Chern, X.-X. Liu, and C.-C. Chang, "Particle plasmons of metal nanospheres: application of multiple scattering approach," Phys. Rev. E **76**, 016609 (2007).
16. S. Riikonen, I. Romero, and F. J. García de Abajo, "Plasmon tunability in metallodielectric metamaterials," Phys. Rev. B **71**, 235104 (2005).
17. S. Lal, S. Link, and N. J. Halas, "Nano-optics from sensing to waveguiding," Nat. Photonics **1**, 641–648 (2007).
18. W.-Y. Chien and T. Szkopek, "Multiple-multipole simulation of optical nearfields in discrete metal nanosphere assemblies," Opt. Express **16**, 1820–1835 (2008).
19. S. A. Maier and H. A. Atwater, "Plasmonics: localization and guiding of electromagnetic energy in metal/dielectric structures," J. Appl. Phys. **98**, 011101 (2005).
20. W. H. Weber and G. W. Ford, "Propagation of optical excitations by dipolar interactions in metal nanoparticle chains," Phys. Rev. B **70**, 125429 (2004).
21. K. H. Fung and C. T. Chan, "Analytical study of the plasmonic modes of a metal nanoparticle circular array," Phys. Rev. B **77**, 205423 (2008).
22. P. C. Waterman, "Symmetry, unitarity, and geometry in electromagnetic scattering," Phys. Rev. D **3**, 825–839 (1971).
23. M. I. Mishchenko, L. D. Travis, and A. A. Lacis, *Scattering, Absorption, and Emission of Light by Small Particles* (Cambridge U. Press, 2002).
24. W. C. Chew, *Waves and Fields in Inhomogeneous Media* (IEEE, 1995).
25. B. Stout, J.-C. Auger, and J. Lafait, "A transfer matrix approach to local field calculations in multiple-scattering problems," J. Mod. Opt. **49**, 2129–2152 (2002).
26. J. Bruning and Y. Lo, "Multiple scattering of EM waves by spheres part I—Multipole expansion and ray-optical solutions," IEEE Trans. Antennas Propag. **19**, 378–390 (1971).
27. J. Bruning and Y. Lo, "Multiple scattering of EM waves by spheres part II—Numerical and experimental results," IEEE Trans. Antennas Propag. **19**, 391–400 (1971).
28. D. W. Mackowski and M. I. Mishchenko, "Calculation of the T matrix and the scattering matrix for ensembles of spheres," J. Opt. Soc. Am. A **13**, 2266–2278 (1996).
29. F. J. García de Abajo, "Multiple scattering of radiation in clusters of dielectrics," Phys. Rev. B **60**, 6086–6102 (1999).
30. M. Quinten and U. Kreibig, "Absorption and elastic scattering of light by particle aggregates," Appl. Opt. **32**, 6173–6182 (1993).
31. B. Stout, J.-C. Auger, and A. Devilez, "Recursive T matrix algorithm for resonant multiple scattering: applications to localized plasmon excitations," J. Opt. Soc. Am. A **25**, 2549–2557 (2008).
32. J. D. Jackson, *Classical Electrodynamics*, 3rd ed. (Wiley, 1999).
33. V. A. Markel, "Antisymmetrical optical states," J. Opt. Soc. Am. B **12**, 1783–1791 (1995).
34. S. Tretyakov, *Analytical Modeling in Applied Electromagnetics* (Artech House, 2003).
35. P. F. Goldsmith, *Quasioptical Systems: Gaussian Beam Quasioptical Propagation and Applications* (IEEE, 1998).
36. B. E. A. Saleh and M. C. Teich, *Fundamentals of Photonics* (Wiley, 1991).
37. L. A. Sweatlock, S. A. Maier, H. A. Atwater, J. J. Penninkhof, and A. Polman, "Highly confined electromagnetic fields in arrays of strongly coupled Ag nanoparticles," Phys. Rev. B **71**, 235408 (2005).
38. A. F. Koenderink and A. Polman, "Complex response and polariton-like dispersion splitting in periodic metal nanoparticle chains," Phys. Rev. B **74**, 033402 (2006).
39. L. Tsang, J. A. Kong, and K.-H. Ding, *Scattering of Electromagnetic Waves: Theories and Applications* (Wiley-Interscience, 2000).